THE JOURNAL OF BIOLOGICAL CHEMISTRY VOL. 291, NO. 39, pp. 20753–20765, September 23, 2016

Structural Insight into the 14-3-3 Protein-dependent Inhibition of Protein Kinase ASK1 (Apoptosis Signal-regulating kinase 1)*[S]

Received for publication, February 26, 2016, and in revised form, July 9, 2016 Published, JBC Papers in Press, August 11, 2016, DOI 10.1074/jbc.M116.724310

Olivia Petrvalska[‡§], Dalibor Kosek[‡§], Zdenek Kukacka[¶], Zdenek Tosner[‡], Petr Man[¶‖], Jaroslav Vecer[**], Petr Herman[**], Veronika Obsilova[§1], and Tomas Obsil[‡§2]

From the [‡]Department of Physical and Macromolecular Chemistry, Faculty of Science, and [‖]Department of Biochemistry, Faculty of Science, Charles University in Prague, 12843 Prague, [§]Institute of Physiology and the [¶]Institute of Microbiology, The Czech Academy of Sciences, 14220 Prague, and the [**]Institute of Physics, Faculty of Mathematics and Physics, Charles University in Prague, 12116 Prague, Czech Republic

Apoptosis signal-regulating kinase 1 (ASK1, also known as MAP3K5), a member of the mitogen-activated protein kinase kinase kinase (MAP3K) family, regulates diverse physiological processes. The activity of ASK1 is triggered by various stress stimuli and is involved in the pathogenesis of cancer, neurodegeneration, inflammation, and diabetes. ASK1 forms a high molecular mass complex whose activity is, under non-stress conditions, suppressed through interaction with thioredoxin and the scaffolding protein 14-3-3. The 14-3-3 protein binds to the phosphorylated Ser-966 motif downstream of the ASK1 kinase domain. The role of 14-3-3 in the inhibition of ASK1 has yet to be elucidated. In this study we performed structural analysis of the complex between the ASK1 kinase domain phosphorylated at Ser-966 (pASK1-CD) and the 14-3-3ζ protein. Small angle x-ray scattering (SAXS) measurements and chemical cross-linking revealed that the pASK1-CD·14-3-3ζ complex is dynamic and conformationally heterogeneous. In addition, structural analysis coupled with the results of phosphorus NMR and time-resolved tryptophan fluorescence measurements suggest that 14-3-3ζ interacts with the kinase domain of ASK1 in close proximity to its active site, thus indicating this interaction might block its accessibility and/or affect its conformation.

Apoptosis signal-regulating kinase 1 (ASK1,[3] also known as MAP3K5), a member of the mitogen-activated protein kinase kinase kinase (MAP3K) family, regulates diverse physiological processes, such as apoptosis, cytokine secretion, or cell differentiation by activating the c-Jun N-terminal kinase and p38 signaling pathways (1). The activity of ASK1, which is triggered by various stress stimuli, is involved in the pathogenesis of cancer, neurodegeneration, inflammation, and diabetes (2). The human ASK1 consists of 1374 amino acid residues with the serine/threonine kinase domain being centrally located and flanked by two coiled-coil (CC) domains. ASK1 forms a high molecular mass complex called ASK1 signalosome under non-stress conditions in which ASK1 homo-oligomerizes through the C-terminal CC domain and interacts with several other proteins including ASK2, thioredoxin, and the 14-3-3 protein (Fig. 1*A*) (3, 4). Thioredoxin presumably prevents homo-oligomerization of ASK1, whereas 14-3-3 binds to the motif located at the C terminus of the kinase domain and suppresses the catalytic activity by unknown mechanism (4–7). In response to oxidative stress, both thioredoxin and 14-3-3 dissociate from ASK1 followed by the homo-oligomerization of ASK1 and the recruitment of tumor necrosis factor receptor-associated factors 2 and 6. This, in turn, accelerates the autophosphorylation of Thr-838 within the activation segment resulting in ASK1 activation (5, 8).

14-3-3 proteins, a family of dimeric proteins ubiquitously expressed in all eukaryotic cells, bind to other proteins by recognizing motifs containing either a phosphorylated serine (Ser(P)) or a phosphorylated threonine (Thr(P)) residue (9). Through these binding interactions, 14-3-3 proteins regulate many biological processes such as cell cycle progression, initiation of apoptosis, control of gene transcription, and neuroendocrine transduction (10–12). 14-3-3 proteins often function as molecular scaffolds that modulate the conformation of their binding partners; if the binding partner is an enzyme, this can affect its catalytic activity. For example, the 14-3-3-dependent activation of serotonin *N*-acetyltransferase (AANAT) and yeast neutral trehalase (Nth1) has been shown to be based on a direct structural change of the catalytic site (13, 14). On the other hand, tyrosine hydroxylase, Raf-1 kinase, and plant plasma membrane H^+-ATPase are regulated through the 14-3-3-dependent modulation of intradomain interactions and/or the quaternary arrangement (15–17).

A functional role of 14-3-3 in the regulation of ASK1 was first suggested by the observation that under non-stress conditions

* This work was supported by the Czech Science Foundation (Project 14–10061S) and the Czech Academy of Sciences (Research Project RVO: 67985823 of the Institute of Physiology). The authors declare that they have no conflicts of interest with the contents of this article.
[S] This article contains supplemental Figs. S1–S3 and Tables S1 and S2.
[1] To whom correspondence may be addressed. Tel.: 420-241062191; E-mail: veronika.obsilova@fgu.cas.cz.
[2] To whom correspondence may be addressed. Tel.: 420-221951303; E-mail: obsil@natur.cuni.cz.
[3] The abbreviations used are: ASK1, apoptosis signal-regulating kinase 1; CC, coiled-coil; CD, catalytic domain; ASK1-CD, catalytic domain of ASK1; AUC, analytical ultracentrifugation; MKK4, mitogen-activated protein kinase kinase 4; pASK1-CD, phosphorylated ASK1-CD; SV, sedimentation velocity; SAXS, small angle x-ray scattering; TEV, tobacco etch virus; PDK1, phosphoinositide-dependent protein kinase 1; BS^2G, bis(sulfosuccinimidyl) glutarate; Bis-Tris, 2-[bis(2-hydroxyethyl)amino]-2-(hydroxymethyl)propane-1,3-diol; sR_g, product of the scattering vector (*s*) and the radius of gyration (*Rg*).

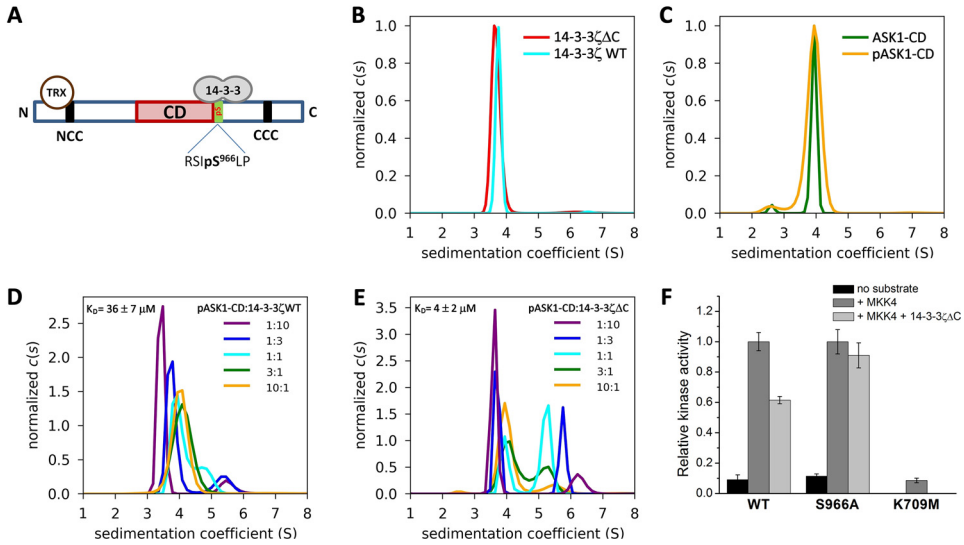

FIGURE 1. **Biophysical characterization of interaction between pASK1-CD and 14-3-3ζ.** *A*, schematic representation of the domain structure of ASK1 with bound thioredoxin (*TRX*) and 14-3-3. *NCC*, N-terminal CC; *CCC*, C-terminal CC; *CD*, catalytic domain; *pS*, phosphoserine. The 14-3-3 binding motif is shown in *green*. *B*, the normalized continuous sedimentation coefficient distributions, *c*(*s*), for 14-3-3ζWT and 14-3-3ζΔC. *C*, the normalized *c*(*s*) distributions for not-phosphorylated ASK1-CD and phosphorylated pASK1-CD. *D*, series of area normalized *c*(*s*) distributions for mixtures of pASK1-CD and for 14-3-3ζWT at various molar ratios. The protein concentration was 18 μM for pASK1-CD and 1.8–180 μM for 14-3-3ζWT. *E*, series of area-normalized *c*(*s*) distributions for mixtures of pASK1-CD and for 14-3-3ζΔC at various molar ratios. The protein concentration was 18 μM for pASK1-CD and 1.8–180 μM for 14-3-3ζΔC. *F*, the catalytic activity of pASK1-CD and the 14-3-3 binding-defective S966A mutant both in the absence and the presence of 14-3-3ζΔC. Human MKK4 (kinase-dead mutant K131A) was used as a substrate. The activities in the presence of 14-3-3ζΔC are normalized to activities in its absence. The activity of kinase-dead ASK1-CD K709M mutant is normalized to the pASK1-CD activity. Results are the means ± S.D., $n = 4$. Specific activities are listed in supplemental Table S1.

14-3-3ζ recognizes a motif containing phosphoserine Ser(P)-966 located at the C terminus of ASK1 kinase domain (Fig. 1*A*) and that the replacement of this residue to alanine dramatically accelerates ASK1-induced cell death (6). It was subsequently shown that the oxidative stress-induced dephosphorylation of Ser(P)-966 is accompanied by an increased autokinase activity of ASK1 and that the 14-3-3 binding-defective mutant ASK1 S966A shows increased both autokinase and transkinase activities (7). However, the molecular mechanism of the 14-3-3-dependent regulation of ASK1 remains elusive.

In this work, we performed structural analysis of the complex between the kinase domain of ASK1 (sequence 659–973) phosphorylated at Ser-966 and the 14-3-3ζ protein using small angle x-ray scattering (SAXS) and chemical cross-linking. In addition, we also investigated whether the 14-3-3ζ binding affects conformation of the active site of ASK1.

Results

Biophysical Characterization of the pASK1-CD·14-3-3ζ Complex—The interaction between pASK1-CD and 14-3-3ζ was first studied using sedimentation velocity (SV) analytical ultracentrifugation (AUC) by analyzing their mixtures at various molar ratios (Fig. 1*D*). The direct modeling of obtained SV AUC data using the Lamm equation revealed the best fit apparent equilibrium dissociation constant (K_D) of 36 ± 7 μM using a Langmuir binding model with one dimer of pASK1-CD interacting with one dimer of 14-3-3ζWT. To increase the stability of the complex, we prepared 14-3-3ζ deleted of its C-terminal 15 residues (14-3-3ζΔC), which binds ligands with significantly higher affinity (17, 18). Indeed, 14-3-3ζΔC showed significantly increased binding affinity for pASK1-CD with the best-fit K_D value of 4 ± 2 μM (Fig. 1*E*). The observed value of $s_{w(20,w)}$ of 6.2S for the complex (based on *c*(*s*) distribution of mixture with highest molar ratio of 14-3-3ζΔC to pASK1-CD shown in *purple* in Fig. 1*E*) corresponds to a M_r of ~121, thus suggesting the 2:2 molar stoichiometry of the complex (a dimer of pASK1-CD bound to a dimer of 14-3-3ζΔC, theoretical M_r 128.9). Considering the significantly improved binding affinity of pASK1-CD for 14-3-3ζΔC compared with WT, we decided to use 14-3-3ζΔC rather than 14-3-3ζWT throughout this work.

14-3-3 Binding Suppresses the Kinase Activity of pASK1-CD—The pASK1-CD used in this study is enzymatically active, allowing us to perform activity measurements to compare the properties of complexed and free pASK1-CD. Human mitogen-activated protein kinase kinase 4 (MKK4), a physiological target of ASK1, was used as a specific substrate. As noticed, the addition of 14-3-3ζΔC suppressed the activity of pASK1-CD relative to the uncomplexed protein by ~40%, whereas no significant decrease in kinase activity was observed for the 14-3-3 binding-defective mutant pASK1-CD S966A (Fig. 1*F*, the specific activities are listed in supplemental Table S1). The 14-3-3ζ-dependent inhibition of pASK1-CD enzyme activity is consistent with data published by Fu and co-workers (6, 7) who showed that ASK1 binding to 14-3-3 caused a significant suppression of ASK1-induced apoptosis through inhibition of its kinase activity.

Characterization of the pASK1-CD·14-3-3ζ Complex by SAXS—The scattering data for 14-3-3ζΔC alone and ASK1-CD alone as well as the pASK1-CD·14-3-3ζΔC complex (mixed with 2:2 molar stoichiometry) were collected at various concentrations (Table 1). The complex was prepared at concentrations of ~60, 95, and 137 μM, thus sufficiently above the K_D (~4 μM). The Guinier plots and the concentration dependence of the forward scattering intensity $I(0)$, the Porod volume V_p, and the radius of gyration R_g were used to assess the data quality.

TABLE 1
Structural parameters determined from SAXS data

Sample	c	c^a	$R_g{}^b$	$R_g{}^c$	D_{max}	$V_p{}^d$	$MM_{exp}{}^e$
	$mg{\cdot}ml^{-1}$	μM	Å	Å	Å	nm^3	kDa
14-3-3ζΔC dimer	17.4	307	27.7 ± 0.1	28.1 ± 0.1	83	80	48.7 ± 0.1
	14.6	258	28.1 ± 0.1	28.3 ± 0.1	85	81	49.7 ± 0.1
	10.4	184	28.3 ± 0.1	28.4 ± 0.1	85	85	49.3 ± 0.2
	7.7	136	28.8 ± 0.1	28.6 ± 0.1	85	87	51.0 ± 0.2
ASK1-CD dimer	9.1	126	33.3 ± 0.1	33.4 ± 0.1	109	121	70.1 ± 0.2
	6.3	87	32.7 ± 0.1	33.1 ± 0.1	109	121	68.2 ± 0.2
	4.1	57	32.6 ± 0.2	32.7 ± 0.1	108	120	67.4 ± 0.3
Complex (2:2)	17.6	136.5	49.0 ± 0.1	49.3 ± 0.1	164	243	133.6 ± 0.4
	12.2	94.6	47.7 ± 0.2	48.1 ± 0.1	161	236	117.4 ± 0.4
	7.7	59.7	47.5 ± 0.3	47.6 ± 0.1	159	232	120.2 ± 0.4

[a] Molar concentration of the 14-3-3ζΔC dimer, ASK1-CD dimer, and the complex with 2:2 stoichiometry.
[b] Calculated using Guinier approximation (40).
[c] Calculated using the program GNOM (41).
[d] The excluded volume of the hydrated particle (the Porod volume).
[e] Molecular weight was estimated by comparison of the forward scattering intensity $I(0)$ with that from the reference solution of bovine serum albumin. Theoretical molecular weights of the 14-3-3ζΔC dimer, ASK1-CD dimer, and the 14-3-3ζΔC·ASK1-CD complex (with 2:2 stoichiometry) are 56.6, 72.2, and 128.9 kDa, respectively.

The Guinier plots were sufficiently linear for all samples except a small deviation at the highest complex concentration (Fig. 2). Because the concentration dependence of R_g and $I(0)$ suggested the presence of repulsive interparticle interactions in samples of 14-3-3ζΔC and attractive interparticle interactions in samples of ASK1-CD and the complex at highest protein concentrations (Table 1), data for 14-3-3ζΔC, ASK1-CD, and the complex at concentrations of 7.7, 6.3, and 12.2 $mg{\cdot}ml^{-1}$, respectively, were selected for *ab initio* shape reconstruction and structural modeling. The apparent M_r of 68.2 and 51 for ASK1-CD and 14-3-3ζΔC, respectively, estimated from $I(0)$ correspond well with the expected M_r of their dimers (Table 1). The estimated M_r of 117.4 for the complex as well as its V_p of 236 nm^3 correspond well to a 2:2 molar stoichiometry (theoretical M_r 128.9), thus corroborating results from SV AUC (for globular proteins, V_p in nm^3 should numerically be ~1.7 times the M_r; Ref. 19).

The shape of the calculated distance distribution function, $P(r)$, suggests that the complex is more extended compared with dimers of ASK1-CD and 14-3-3ζΔC as its $P(r)$ function shows longer intraparticle distances and a significantly larger maximum particle distance (D_{max}) (Fig. 3*A* and Table 1). The normalized Kratky plots for both 14-3-3ζΔC and ASK1-CD show bell-shaped curves with a maximum at $sR_g = 1.7$ consistent with folded molecules (Fig. 3*B*) (20). However, the normalized Kratky plot of the complex indicates an increase in the degree of the flexibility exhibited by the complex as indicated by the more gradual decrease of the curve toward zero at higher sR_g and a maximum at $sR_g = 2.2$.

The superposition of *ab initio* molecular envelope of 14-3-3ζΔC with the crystal structure of 14-3-3ζ (21) revealed correct reproduction of its molecular shape (Fig. 4*A*). The theoretical scattering curve calculated from the crystal structure fits the experimental data reasonably well (Fig. 4*B*, $\chi = 0.97$, $R_g = 29.2$ Å). The *ab initio* shape reconstruction statistics are listed in Table 2. The superposition of *ab initio* molecular envelope of ASK1-CD with the AllosMod model of ASK1-CD (659–973) also showed correct reproduction of the shape and fit well the experimental SAXS data (Fig. 4, *C* and *D*, $\chi = 1.00$, $R_g = 33.3$ Å). The molecular envelope of the pASK1-CD·14-3-3ζΔC complex is, as expected, significantly more extended compared with ASK1-CD and 14-3-3ζΔC alone, and its shape, with one side being narrower than the other, suggests that protein components are arranged asymmetrically (Fig. 4*E*).

Chemical Cross-linking of the pASK1-CD·14-3-3ζΔC Complex—The chemical cross-linking experiments were performed to obtain distance restraints for structural modeling of the complex. Identified intermolecular cross-links connecting four different regions of pASK1-CD with four different regions of 14-3-3ζΔC are listed in Table 3. In several cases we were unable to identify the exact cross-linked residue, as the corresponding peptides contained multiple, usually closely located, lysine residues. Cross-link #1 connects the N-terminal amino group of Met-658 of pASK1-CD and the N-terminal part of helix H6 of 14-3-3ζΔC containing two lysines, Lys-122 and Lys-138 (supplemental Fig. S2). Cross-link #2 was identified between the C terminus of helix αC from the N-lobe of pASK1-CD containing Lys-730 (or Lys-733) and the C terminus of helix H6 of 14-3-3ζΔC containing Lys-158. Cross-link #3 connects Lys-925 from the loop between helices αH and αI of the C-lobe of pASK1-CD and Lys-85 from the helix H4 of 14-3-3ζΔC. Cross-link #4 connects the C-terminal part of pASK1-CD containing lysines Lys-944, Lys-945, and Lys-946 and the C terminus of helix H3 of 14-3-3ζΔC containing Lys-68. The last cross-link was identified between lysines Lys-944–Lys-946 of pASK1-CD and residue Lys-120 from the helix H5 of 14-3-3ζΔC. However, this cross-link was also observed for the mixture of non-phosphorylated ASK1-CD and thus was not used in structural modeling of the complex as it likely results from unspecific interaction between ASK1-CD and 14-3-3ζΔC.

All-Atom Modeling of the pASK1-CD·14-3-3ζΔC Complex—The all-atom modeling of the pASK1-CD·14-3-3ζΔC complex was first performed using the AllosMod-FoXS method (22, 23). The best-scoring single-state AllosMod model fits the SAXS data with $\chi = 1.66$ and shows the C-lobe of one protomer of ASK1-CD interacting with α-helices H4 and H6 of 14-3-3ζ outside its central channel through a relatively small binding interface (Fig. 5, *A* and *B*). Although this model satisfies three identified cross-links within a distance threshold of 30 Å and shows a reasonable agreement with the *ab initio* molecular envelope (Fig. 5*C*), calculated χ value together with theoretical values of R_g and D_{max} (43.1 and 156.7 Å, respectively), which are significantly smaller compared with values obtained from the SAXS data (Table 1), suggested this model does not reproduce the experimental SAXS data correctly.

Because normalized Kratky plot indicated an increased degree of flexibility exhibited by the complex (Fig. 3*B*), a multistate modeling of the complex for up to five states using the MultiFoXS method that enables modeling of conformationally heterogeneous systems was performed next (24, 25). The resulting best-scoring model is based on a weighted combination of three states and provides a significantly improved fit to the SAXS data with χ of 0.97 as well as agreement with cross-linking data within a distance threshold of 30 Å (Fig. 6). Combinations of two, four, or five states did not yield any solution that would better describe the SAXS data compared with the three-state model. The model consists of two compact states with population weights of 43% ($R_g = 41.6$ Å, $D_{max} = 153.5$ Å)

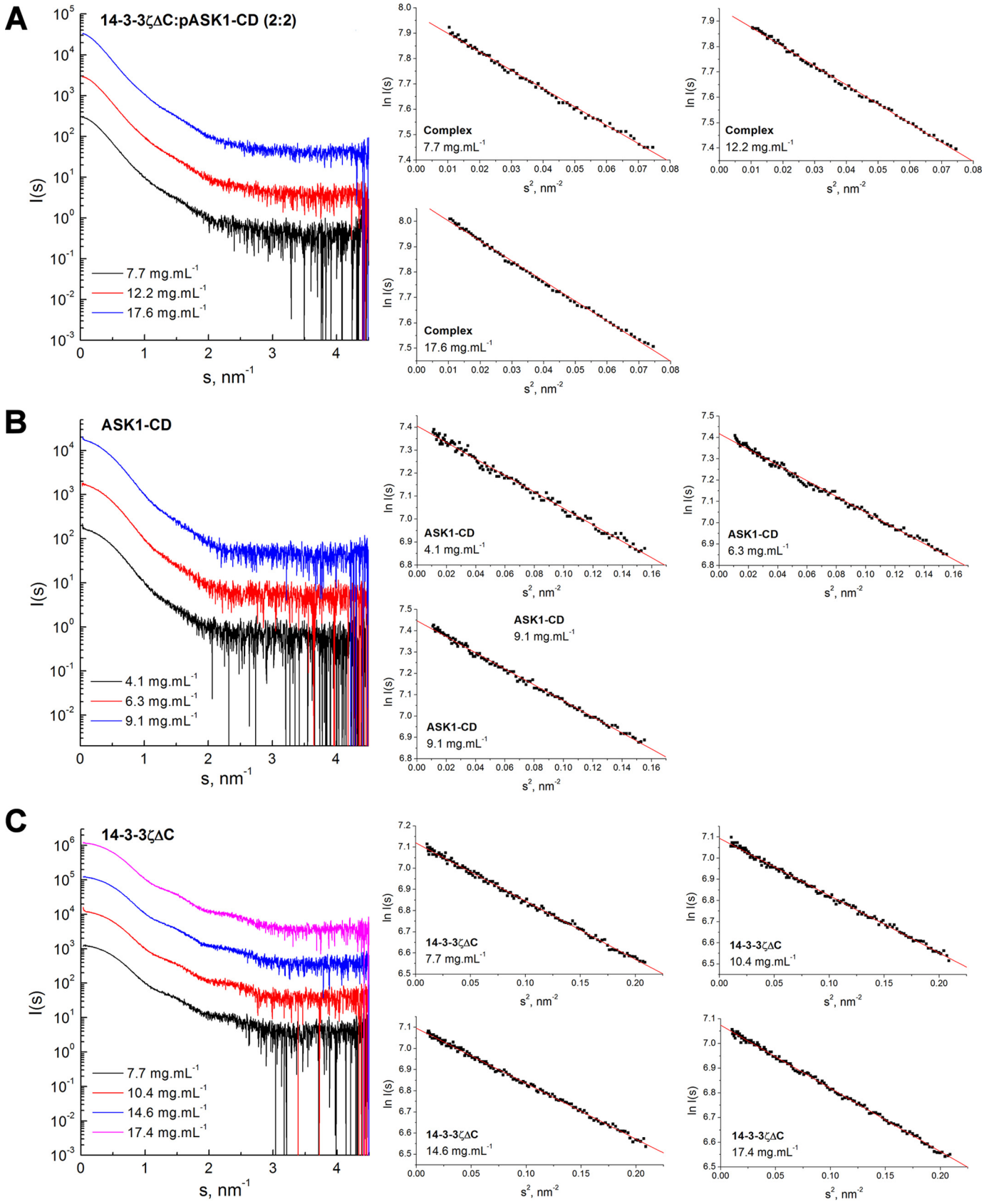

FIGURE 2. **SAXS data of ASK1-CD, 14-3-3ζΔC, and the pASK1-CD·14-3-3ζΔC complex.** Scattering intensity as a function of the scattering vector s ($s = 4\pi\sin(\theta)/\lambda$, where 2θ is the scattering angle, and λ is the wavelength) and Guinier plots ($\ln I(s)$ *versus* s^2) of all measured samples. *A*, 14-3-3ζΔC alone. *B*, ASK1-CD alone. *C*, the pASK1-CD·14-3-3ζΔC complex (mixed with 2:2 stoichiometry). Scattering curves are shown with offsets for better clarity.

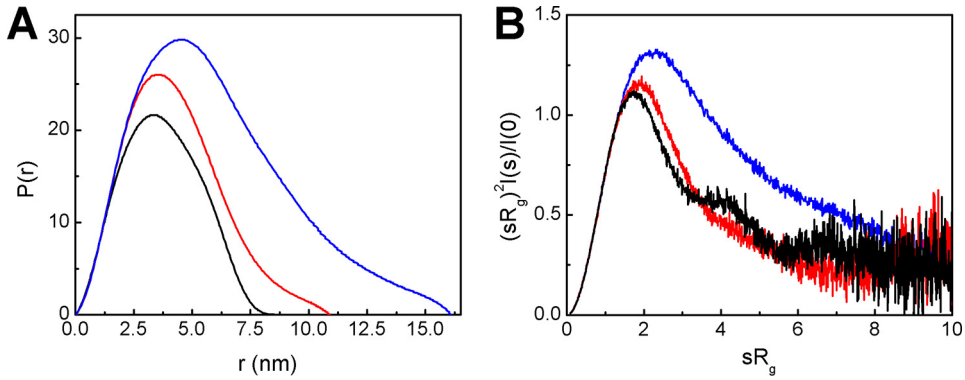

FIGURE 3. **SAXS analysis of ASK1-CD, 14-3-3ζΔC, and the pASK1-CD·14-3-3ζΔC complex.** *A*, distance distribution function *P*(*r*) calculated from scattering data using the program GNOM (41). *B*, normalized Kratky plots of 14-3-3ζΔC (*black*), ASK1-CD (*red*), and the pASK1-CD·14-3-3ζΔC complex (*blue*).

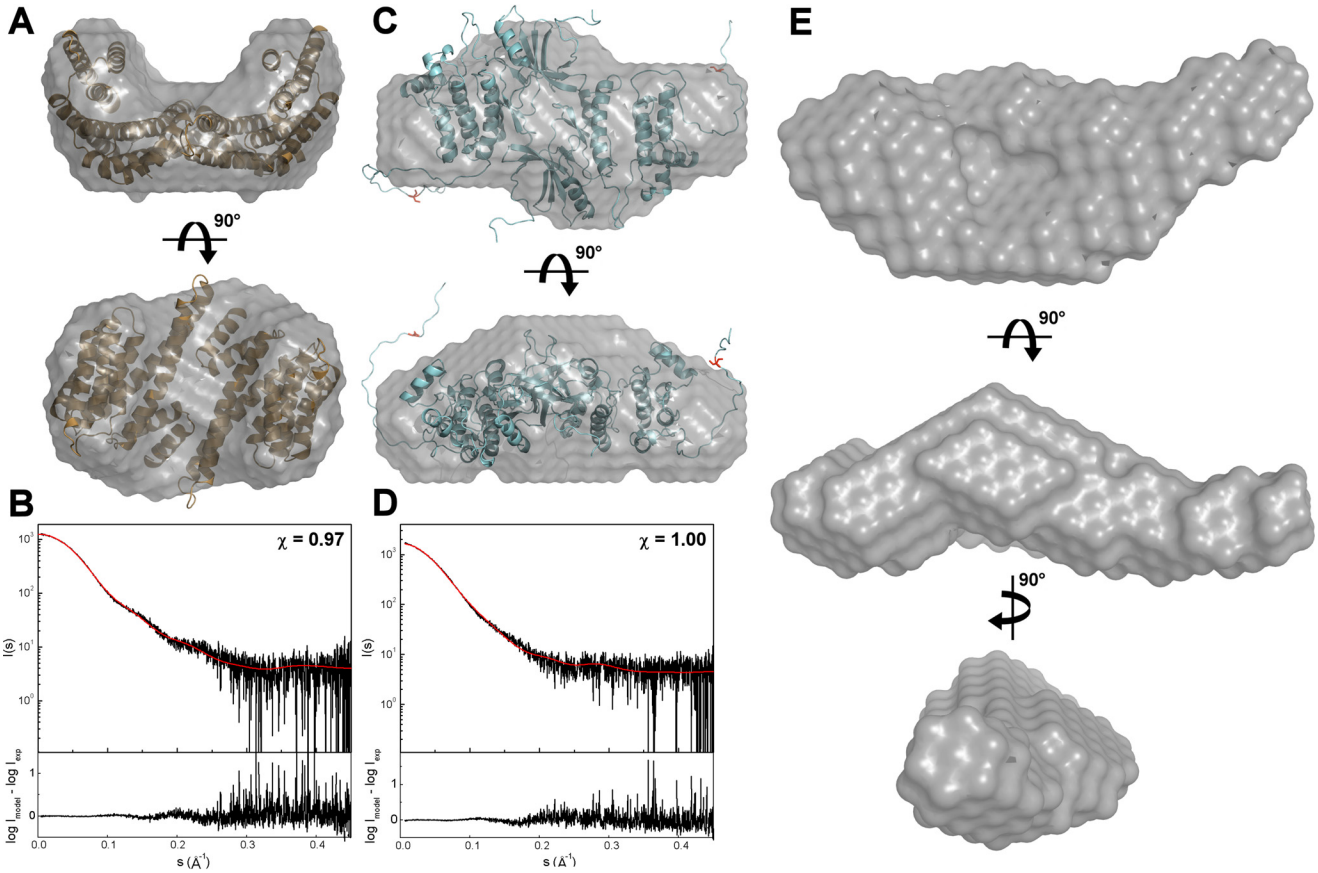

FIGURE 4. **Shape reconstructions calculated from the experimental SAXS data.** *A*, *ab initio* shape reconstruction of 14-3-3ζΔC calculated from SAXS data (represented as a *gray envelope*) with a superimposed crystal structure of 14-3-3ζ (21). *B*, comparison of the calculated scattering curve of the crystal structure of 14-3-3ζ (red line) with the experimental scattering data (*black line*). *C*, *ab initio* shape reconstruction of ASK1-CD calculated from SAXS data with superimposed AllosMod model of ASK1-CD (659–973). *D*, comparison of the calculated scattering curve of ASK1-CD (659–973) model (*red line*) with the experimental scattering data (*black line*). *E*, *ab initio* reconstruction of the pASK1-CD·14-3-3ζΔC complex calculated from SAXS data. The *ab initio* shape reconstructions were performed using the program DAMMIF (43). Calculated molecular envelopes were aligned to structural models using the program SUPCOMB (45). Theoretical scattering curves were calculated from structural models and fitted to experimental data using CRYSOL (46).

and 18% (R_g = 37.9 Å, D_{max} = 139.0 Å) where the C-lobe of one protomer of ASK1-CD faces either the α-helix H6 or loops between helices H2-H3 and H4-H5 of 14-3-3ζ and one extended state with the population weight of 39% (R_g = 56.6 Å, D_{max} = 214.3 Å), where 14-3-3ζ and ASK1-CD are separated but still connected through the C-terminal segment of ASK1-CD. A significantly better agreement of this three-state model with the SAXS data compared with the single-state AllosMod model suggested that the pASK1-CD·14-3-3ζΔC complex is conformationally heterogeneous in solution with both proteins sampling various mutual orientations.

The 14-3-3 Binding Affects Local Environment and Dynamics of Thr(P)-838 and Thr(P)-842 in the Activation Segment of pASK1-CD—Structural modeling suggested that 14-3-3ζ interacts with the C-lobe of pASK1-CD in close proximity to both the active site and activation segment (Fig. 7). This brings up the possibility that the 14-3-3 binding might affect conformation of this region either directly or indirectly. Because the acti-

TABLE 2

***Ab initio* shape reconstruction statistics**

Ab initio shape reconstructions were performed using the program DAMMIF (43). *c*, concentration.

Parameter	14-3-3ζΔC	ASK1-CD	Complex (2:2)
c (mg·ml^{-1})	7.7	6.3	12.2
Angular range (nm^{-1})	0.11-3.08	0.17–2.44	0.12–2.40
Real space range (nm^{-1})	0–8.5	0–10.9	0–16.1
GNOM total estimate	0.78	0.56	0.51
Symmetry	P2	P2	P1
χ^a	0.80	0.90–0.93	0.98–1.01
Number of models averaged/total	14/15	13/15	14/15
Damaver NSD	0.79	0.78	0.89

[a] Discrepancy between the simulated scattering curve and the experimental data.

vation segment contains two autophosphorylation sites that are phosphorylated in our recombinant protein (Thr(P)-838 and Thr(P)-842, supplemental Fig. S1), ^{31}P NMR experiments were performed to study structural changes of this region upon the 14-3-3ζ binding. The ^{31}P NMR spectrum of pASK1-CD alone showed a strong and narrow resonance at 4.6 ppm and 2 overlapping resonances at 3– 4.25 ppm (Fig. 8). All these resonances lie within the range ~3–5 ppm expected for chemical shifts of Ser(P) and Thr(P) at neutral pH (26). The spectrum of the 14-3-3 binding-defective mutant pASK1-CD S966A alone contains only resonances at 3– 4.25 ppm, thus strongly suggesting that resonance at 4.6 ppm corresponds to ^{31}P nuclei of Ser(P)-966. The narrow line width of this resonance likely reflects the high flexibility of the C-terminal segment. Two broad overlapping resonances at 3– 4.25 ppm likely correspond to ^{31}P nuclei of autophosphorylation sites Thr(P)-838 and Thr(P)-842, the only other phospho-residues present in our recombinant pASK1-CD (the third autophosphorylation site Thr-813 was phosphorylated negligibly, supplemental Fig. S1, *A–C*). The spectrum of 14-3-3ζΔC alone exhibited a single resonance at 5.25 ppm, suggesting the presence of one weakly phosphorylated site in the recombinant protein. The addition of 14-3-3ζΔC to pASK1-CD significantly suppressed resonance of Ser(P)-966 at 4.6 ppm, likely due to its binding into the ligand binding groove of 14-3-3, and changed ratio of intensities of Thr(P)-838 and Thr(P)-842 resonances at 3– 4.25 ppm. On the other hand and as expected, no changes were observed in the spectrum of the 14-3-3 binding-defective S966A mutant in the presence of 14-3-3ζΔC. This supports the hypothesis that the 14-3-3 binding affects conformation of the activation segment of pASK1-CD and so the local environment and dynamics of Thr(P)-838 and Thr(P)-842 phosphate groups. Furthermore, strong suppression of resonance of Ser(P)-966 at 4.6 ppm in the presence of 14-3-3 indicates that the exchange between free and bound states of pASK1-CD occurs at an intermediate NMR time scale and involves both protomers of the pASK1-CD dimer.

The 14-3-3 Binding Changes Fluorescence Properties of Tryptophan at Position 823 in the Activation Segment of pASK1-CD—Next, time-resolved tryptophan fluorescence experiments were performed to further confirm the 14-3-3ζ binding-induced structural changes within the active site of pASK1CD. To this end, two ASK1-CD mutants containing a single Trp residue at two different positions (823 and 839) within the activation segment were designed. Two tryptophans present in the sequence of ASK1-CD (Trp-770 and Trp-865) were mutated to Phe, and a single tryptophan was introduced at positions 823 and 839 by mutating the corresponding Phe to Trp. However, only the mutant containing single Trp at position 823 possessed sufficient solubility and stability for further experiments. We also generated mutants containing single Trp-770 or Trp-865 (by mutating the other Trp to Phe); nonetheless, only the mutant containing Trp-770 was soluble and stable. Residue Trp-770 is located at the C terminus of helix αD (Fig. 7); thus, this mutant was used to monitor structural changes in this part of ASK1-CD molecule. The stability of prepared mutants was checked by measuring the thermally induced protein denaturation using differential scanning fluorimetry. No significant differences in the temperature of the unfolding transition (T_m) were observed for prepared ASK1-CD mutants (supplemental Table S2). The fluorescently silent human 14-3-3ζnoW missing all Trp residues was used in all tryptophan fluorescence measurements (27). Fluorescence decay measurements revealed that the complex formation significantly decreased the mean-excited state lifetime τ_{mean} of Trp-823 from 5.8 to 5.4 ns (Table 4). The τ_{mean} shortening is clearly visible in the raw data presented in Fig. 9 where the difference between fluorescence decays in the presence and absence of 14-3-3ζnoW is visibly above the data noise level. As can be noticed from the lifetime distribution analysis in Fig. 10, the decrease in τ_{mean} is caused mainly by the binding-induced shortening of the two longest lifetime peaks representing together almost 70% of the total fluorescence intensity. These two peaks dominate the mean excited state lifetime, as $\tau_{mean} = \Sigma_i(f_i\tau_i)$, where f_i represents intensity fraction of the ith lifetime component τ_i (28). Statistical significance of the observed difference is supported by the bootstrap confidence-interval analysis (29) presented in supplemental Fig. S3. The binding effect of 14-3-3ζnoW on τ_{mean} of Trp-770 was found to be considerably weaker (Table 4). The suppression of τ_{mean} indicates a significant 14-3-3ζ binding-induced increase in polarity in the close vicinity of Trp-823 and/or change in quenching interactions upon the complex formation. This result corroborates the hypothesis that the 14-3-3ζ binding affects conformation of the activation segment of pASK1-CD.

Analysis of the time-resolved emission anisotropy decays of pASK1-CD alone revealed three correlation times, one short (ϕ_1 = 2.5 ns), the second close to 18 ns (ϕ_3) and the third very long unresolved ($\phi_4 > 200$ ns). Although the ϕ_1 reflects fast segmental motions, the ϕ_3 closely corresponds to the rotation of globular protein with M_r ~70 (28) and can, therefore, be assigned to the overall rotational motion of pASK1-CD. The long correlation time ϕ_4 cannot be resolved with short Trp fluorescence lifetime and likely reflects a presence of some protein aggregates. For both mutants, the complex formation increased the correlation time to values corresponding to the overall rotational motion of protein with M_r of 110–150 (28), thus reflecting the higher molecular mass of the complex. Compared with pASK1-CD alone, complex formation resulted in an appearance of a new correlation time component (ϕ_2), which is too long to be attributed to segmental motions. It rather reflects domain motions of pASK1-CD within the complex and/or the complex asymmetricity and structural heterogeneity as has been suggested by SAXS (Figs. 3*B* and 6).

TABLE 3
Intermolecular cross-links between ASK1-CD and 14-3-3ζΔC obtained with BS^2G

Cross-link number	Cross-linked peptides		Cross-linked residues	Observed mass	Error
	ASK1-CD	14-3-3ζΔC	ASK1-CD-14-3-3ζΔC		
					ppm
1[a]	658–659	121–139	Met-658[b]- (Lys-122 or Lys-138)	2594.2297	3.3
2	718–735	158–167	(Lys-730 or Lys-733)-Lys-158	3539.8599	2.8
3	918–926	84–91	Lys-925--Lys-85	2219.0708	2.5
4	944–950	61–75	(Lys-944 or Lys-945 or Lys-946)-Lys-68	2585.4470	1.6
5	944–945[c]	116–122	(Lys-944 or Lys-945)-Lys-120	1298.7528	1.3
6[d]	944–945[c]	116–122	(Lys-944 or Lys-945)-Lys-120	1298.7533	0.9

[a] Cross-links 1–5 were observed for the mixture of pASK1-CD and 14-3-3ζΔC.
[b] Residue Met-658 is the N-terminal Met residue of ASK1-CD construct.
[c] Lys-944–Lys-945 or Lys-945–Lys-946 (from the ASK1 region ^{943}KKKK^{946}).
[d] This cross-link was observed for the mixture of not-phosphorylated ASK1-CD and 14-3-3ζΔC.

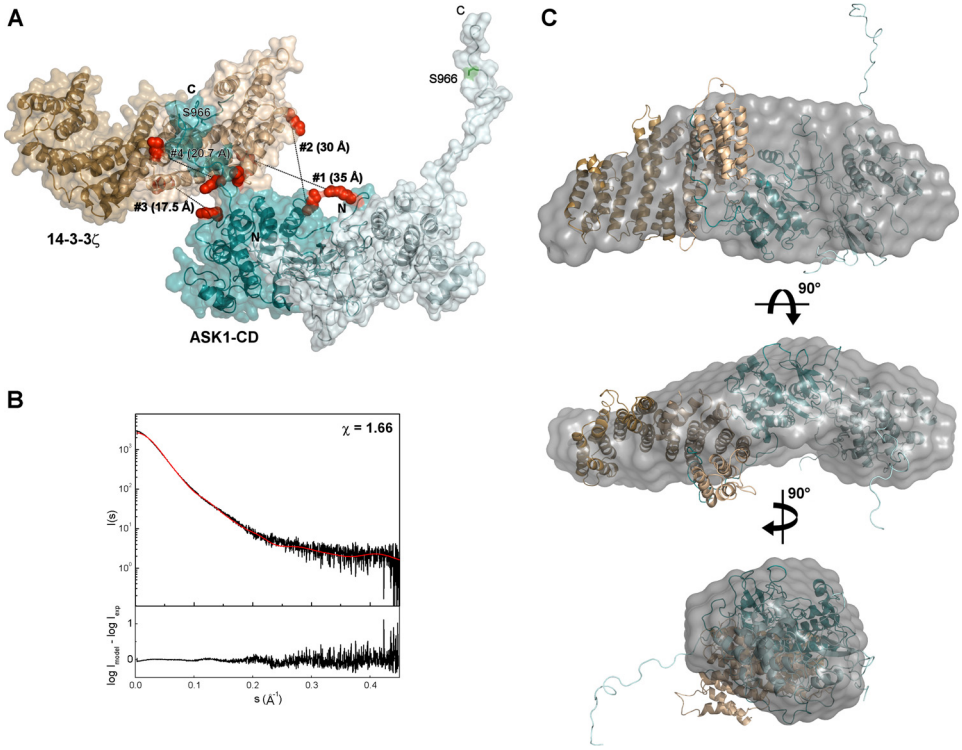

FIGURE 5. **Single-state model of the pASK1-CD·14-3-3ζ complex.** *A*, the best-scoring single-state model of the pASK1-CD·14-3-3ζ complex calculated using the AllosMod-FoXS server (22, 23). The 14-3-3ζ is shown in *brown*, and ASK1-CD is shown in *cyan* (each protomer is shown in a different shade). Intermolecular cross-links are labeled according to Table 3 (cross-linked residues are shown in *red*), and their distances are shown in *parenthesis*. As can be noticed, the model satisfies three identified cross-links within a distance threshold of 30 Å. *B*, comparison of the calculated scattering curve of the model (*red line*) with the experimental scattering data (*black line*). Theoretical scattering curve was calculated and fitted to experimental data using FoXS (47). *C*, *ab initio* molecular envelope of the pASK1-CD·14-3-3ζ complex calculated from SAXS data (represented as a *gray envelope*) with superimposed single-state model of the complex. Calculated molecular envelope was aligned to structural model using the program SUPCOMB (45).

Discussion

The location of the 14-3-3 binding motif close to the kinase domain of ASK1 (25 amino acid residues downstream of its C terminus) raised the possibility that the 14-3-3 protein binding might modulate the structure of this domain and/or the accessibility of its active site, as has been suggested for other enzymes regulated in the 14-3-3-dependent manner (13, 14). The aim of this study was to investigate this hypothesis by performing structural analysis of the complex between 14-3-3ζ and pASK1-CD. The *ab initio* shape reconstruction of the complex from the SAXS data suggested that dimers of pASK1-CD and 14-3-3ζΔC are arranged asymmetrically and not, as one would expect, symmetrically, as both proteins form dimers with 2-fold symmetry. The SAXS data analysis also suggested that the molecule of the pASK1-CD·14-3-3ζΔC complex consists of several rigid domains that are tethered by linkers with rather compact conformation (Fig. 3*B*), thus resembling, for example, the NADPH oxidase activator $p47^{phox}$ (20, 30). This was further corroborated by the all-atom structural modeling, which revealed that only a model based on a weighted combination of multiple structural states can correctly reproduce both the SAXS and cross-linking data (Fig. 6). This suggested that the complex between 14-3-3ζ and pASK1-CD is dynamic and conformationally heterogeneous with both proteins sampling various mutual orientations. The absence of the large and well defined contact interface between 14-3-3ζ and pASK1-CD, besides interactions between the 14-3-3ζ ligand binding groove and the phosphorylated 14-3-3 binding motif of pASK1-CD, corresponds well with the weak binding affinity determined using SV AUC (Fig. 1, *D* and *E*) (31).

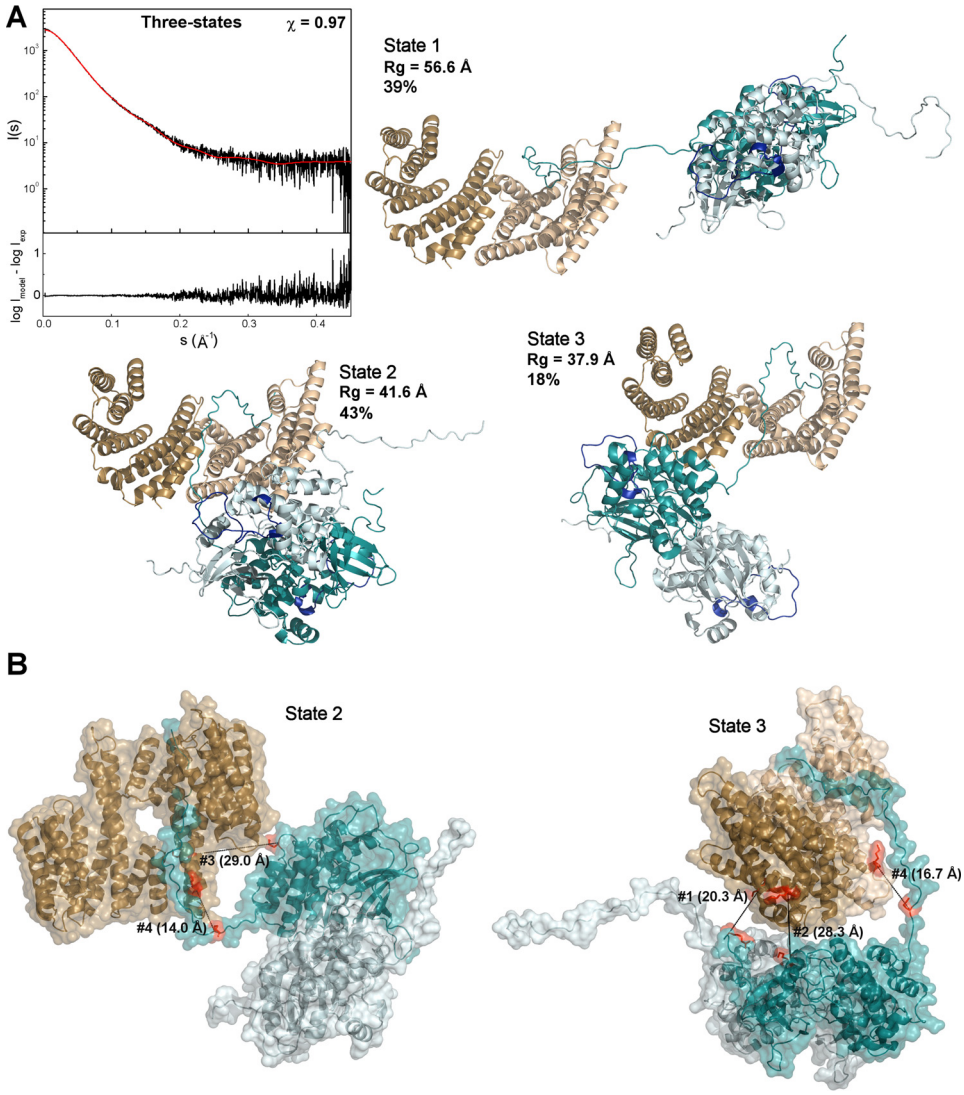

FIGURE 6. **Multistate model of the pASK1-CD·14-3-3ζ complex.** *A*, the best scoring three-state model of the 14-3-3ζ·ASK1-CD complex contains two compact states with population weights of 43% (R_g = 41.6 Å, D_{max} = 153.5 Å) and 18% (R_g = 37.9 Å, D_{max} = 139.0 Å) and one extended state with the population weight of 39% (R_g = 56.6 Å, D_{max} = 214.3 Å). The 14-3-3ζ is shown in *brown*; ASK1-CD is shown in *cyan* (each protomer is shown in a different shade). The activation segment of ASK1-CD is shown in *dark blue*. The weighted combination of these three states (*red line*) agree well with experimental SAXS data (*black line*, χ = 0.97). Multistate model analysis against the SAXS data was performed using the MultiFoXS server (24, 25). *B*, models corresponding to states 2 and 3 from the best scoring three-state model of the 14-3-3ζ·ASK1-CD complex satisfy the cross-linking data within a distance threshold of 30 Å. Intermolecular cross-links are labeled according to Table 3 (cross-linked residues are shown in *red*), and their distances are shown in *parentheses*.

The suggested structural model also explains the observed stoichiometry of the complex in which one protomer of 14-3-3ζ dimer interacts with one protomer of pASK1-CD dimer, thus leaving one ligand binding groove of the 14-3-3ζ dimer and one 14-3-3 binding motif of the pASK1-CD dimer-free (Figs. 5 and 6). However, the formation of complexes with higher stoichiometries has not been observed even in the presence of large excess of one component (Fig. 1, *D* and *E*). The sampling of various conformational states likely causes steric hindrances, thus blocking the formation of complexes with higher binding stoichiometries. This, on the other hand, does not rule out the possibility that within the multiprotein ASK1 signalosome the 14-3-3 dimer interacts simultaneously with ASK1 and yet another protein, *e.g.* ASK2 (4). In addition, the suggested structural model of the pASK1-CD·14-3-3ζ complex also explains the observed partial inhibition of pASK1-CD activity in the presence of 14-3-3 (Fig. 1*F*) as only one protomer of pASK1-CD is bound to, and thus, inhibited by 14-3-3.

Structural analysis also indicated that 14-3-3ζ interacts not only with the phosphorylated motif containing Ser(P)-966 but also with several regions from the C-lobe of pASK1-CD in the vicinity of the active site (Fig. 7). Although these contacts seem transient, it is reasonable to speculate they could affect, either directly or indirectly, the structure of the active site and/or its accessibility as has been observed for other kinases regulated through protein-protein interactions. For example, the cyclin-dependent kinase 2 is activated through the cyclin A-induced conformational change that realigns active site residues and, together with the conformational change of the activation segment, relieves the blockade of the active site (32). On the other hand, the inhibition of PKA is based on direct interaction of the activation segment with the regulatory subunit (33). Yet

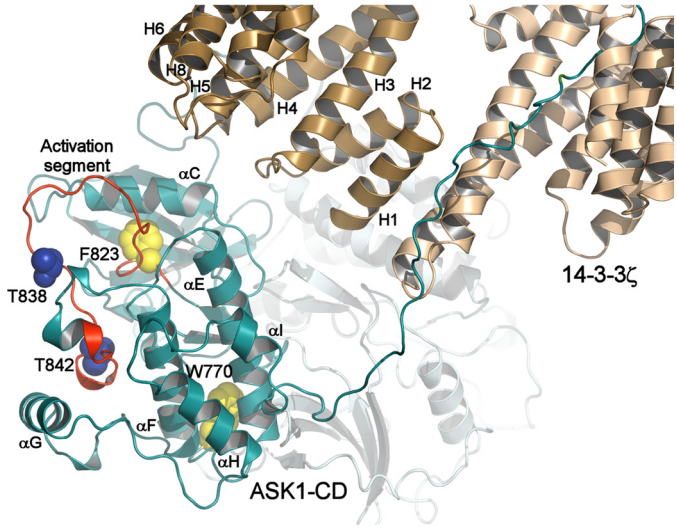

FIGURE 7. **Interactions between the C-lobe of pASK1-CD and 14-3-3ζ.** Shown is a close-up view of the interaction between pASK1-CD and 14-3-3ζ from the model corresponding to state 3 from the best scoring 3-state model of the complex obtained using the MultiFoXS server. The activation segment is shown in *red*. The autophosphorylation sites Thr-838 and Thr-842 are shown in *dark blue*. Residues Trp-770 and Phe-823 are shown in *yellow*.

another example is the inhibition of p38α kinase by MAPK-activated protein kinase 2, which blocks access to the p38α active site upon the complex formation (34). Results of ^{31}P NMR and time-resolved tryptophan fluorescence measurements (Figs. 8–10 and Table 4) suggested that the 14-3-3ζ binding affects conformation of the activation segment of pASK1-CD, thus corroborating the hypothesis that the 14-3-3ζ protein interacts with pASK1-CD in close proximity to its active site. This suggests that the 14-3-3ζ protein might inhibit pASK1-CD through several mechanisms including structural modulation of its active site, the steric blocking of Thr-838 phosphorylation, and/or the blocking of interaction between ASK1 and its substrates.

Experimental Procedures

Preparation of the Catalytic Domain of ASK1—DNA encoding the catalytic domain and the 14-3-3 binding motif of human ASK1 (residues 659–973) with the His_6 tag and TEV cleavage site at the C terminus was ligated into pST39 vector using XbaI and BamHI restriction sites. The 3-phosphoinositide-dependent protein kinase 1 (PDK1) is the only protein kinase shown to phosphorylate Ser-966 of ASK1 so far (35). The activity of commercially available PDK1, however, did not allow for preparation of milligram quantities of ASK1 (659–973) stoichiometrically phosphorylated at Ser-966 needed for structural studies. Therefore residue Ser-964 was mutated to Arg, thereby making Ser-966 a substrate for the cAMP-dependent protein kinase (PKA). The mutant S964R (denoted as ASK1-CD throughout this work) as well as all other mutants of ASK1-CD were generated using the QuikChange site-directed mutagenesis kit (Stratagene), and mutations were confirmed by sequencing. ASK1-CD was expressed by leakage expression at 25 °C for 18 h and purified from *Escherichia coli* Rosetta™ (DE3) cells using Chelating Sepharose® Fast Flow (GE Healthcare) according to the standard protocol. The His_6 tag was cleaved by incubation with TEV protease (1 mg of TEV/30 mg of fusion protein) at 4 °C for 12 h during dialysis against buffer containing 50 mM Tris-HCl (pH 7.5), 200 mM NaCl, 5 mM EDTA, and 2 mM β-mercaptoethanol. The final purification step was size-exclusion chromatography on a Superdex 200 HiLoad 26/60 column (GE Healthcare) in buffer containing 50 mM Tris-HCl (pH 7.5), 200 mM NaCl, 1 mM EDTA, 5 mM DTT, and 10% (w/v) glycerol.

Phosphorylation of ASK1 (659–973)—ASK1-CD (1 mg·ml^{-1}) was phosphorylated by incubation at 30 °C for 2 h and then overnight at 4 °C with 100 units of PKA (Promega) per mg of protein in the presence of 0.75 mM ATP and 12 mM $MgCl_2$. After the phosphorylation, ATP was removed using size-exclusion chromatography. The result of phosphorylation reaction was verified using HPLC-MS. The HPLC-MS analyses confirmed almost stoichiometric phosphorylation of Ser-966 (supplemental Fig. S1*D*) and a significant autophosphorylation of Thr-838 and Thr-842 for the majority of samples (supplemental Fig. S1, *B* and *C*). If incomplete phosphorylation of Ser-966 was observed, then this procedure was repeated.

HPLC-MS Analysis—HPLC-MS was performed on a HPLC 1200 (Agilent Technologies, Waldbronn, Germany) connected to an electrospray ionization Fourier transform ion cyclotron MS (15T SolariX XR). Proteins were digested online on a pepsin column (66-μl bed volume, flow rate 100 μl·min^{-1}), and the peptides were trapped on a Peptide MicroTrap (Michrom Bioresources, Auburn, CA). After complete desalting they were separated on a C18 reversed phase column (1 × 100 mm, Jupiter, Phenomenex) using a linear gradient of 10–35% solvent B in solvent A in 20 min, where solvent A was 2% acetonitrile and 0.4% formic acid in water, and solvent B was 95% acetonitrile, 5% water, and 0.4% formic acid. Peptides were identified by MASCOT against a database containing a sequence of human ASK1 (the only allowed partial modification was Ser/Thr phosphorylation). Data were analyzed using the program DataAnalysis version 4.2 (Bruker Daltonics).

Preparation of 14-3-3ζ—The 14-3-3 protein wild-type (human isoform ζ), the C-terminally truncated version 14-3-3ζΔC (residues 1–230), and 14-3-3ζnoW were prepared as described previously (13).

Preparation of Kinase-dead MKK4—DNA encoding human MKK4 (also known as MAP2K4/SEK1) was a gift from Dustin Maly (Addgene plasmid #29579) (36). The kinase-dead mutant K131A was generated using the QuikChange site-directed mutagenesis kit (Stratagene), and the mutation was confirmed by sequencing. The His_6-GST-tagged protein was expressed by isopropyl 1-thio-β-D-galactopyranoside induction for 12 h at 25 °C and purified from *E. coli* BL21(DE3) using Chelating Sepharose® Fast Flow (GE Healthcare) according to the standard protocol. The final purification step was size-exclusion chromatography on a Superdex 200 HiLoad 26/60 column (GE Healthcare) in buffer containing 20 mM Tris-HCl (pH 7.5), 150 mM NaCl, 2 mM EDTA, 5 mM DTT, and 10% (w/v) glycerol.

Differential Scanning Fluorimetry—The thermofluor assay was performed using a real-time PCR LightCycler 480 II (Roche Applied Science) as described previously (14). The proteins at a concentration of 0.3 mg·ml^{-1} were tested in the presence of 8× concentrated Sypro Orange (Sigma) in a total reaction volume of 25 μl.

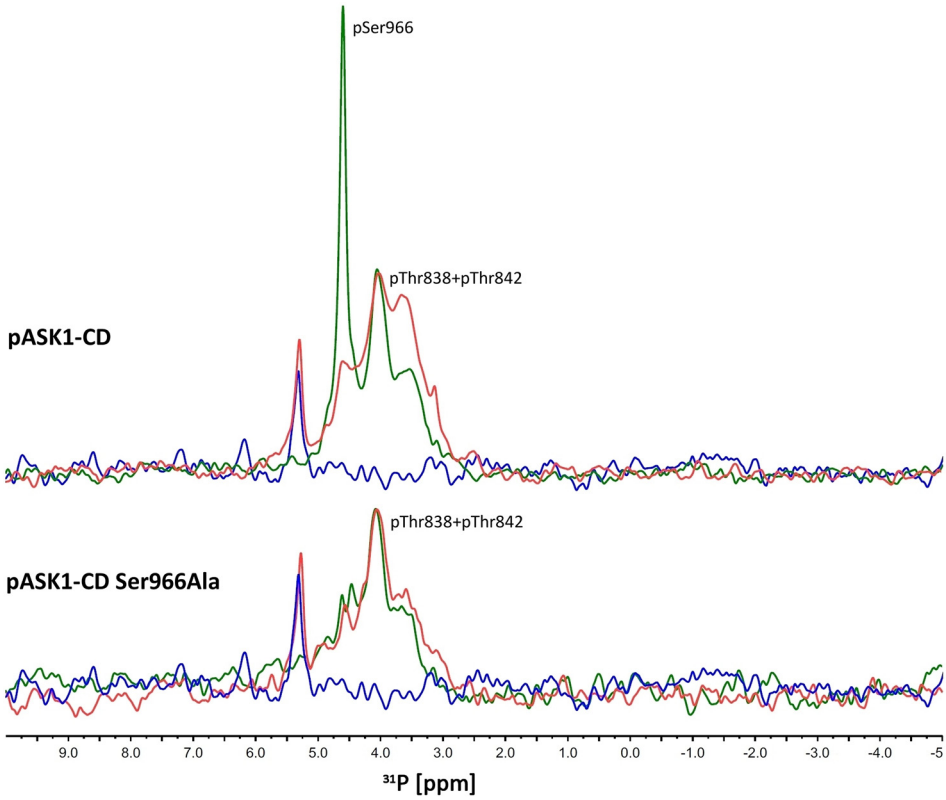

FIGURE 8. **Phosphorus NMR measurements.** ^{31}P NMR measurements are shown of pASK1-CD and pASK1-CD S966A mutants in the absence (*green traces*) and the presence of 14-3-3ζΔC (*red traces*). The spectrum of 14-3-3ζΔC alone is shown in *blue*. The data were collected at 23 °C and 202.4 MHz ^{31}P resonance frequency.

TABLE 4

Summary of time-resolved tryptophan fluorescence measurements of pASK1-CD

pASK1-CD	τ_{mean} [a]	ϕ_1	β_1 [b]	ϕ_2	β_2	ϕ_3	β_3	ϕ_4	β_4
	ns	*ns*		*ns*		*ns*		*ns*	
Single Trp mutant									
Trp-823[c]	5.8	2.5	0.04			17.8	0.11	200	0.03
Trp-823 + 14-3-3ζnoTrp-	5.4	3.3	0.04	8.5	0.01	37.5	0.12		
Trp-770[d]	5.7	2.5	0.04			17.1	0.12	200	0.04
Trp-770 + 14-3-3ζnoW	5.5	1.6	0.03	10.2	0.07	41.1	0.09		

[a] Mean lifetimes were calculated as $\tau_{mean} = \Sigma_i f_i \tau_i$, where f_i is an intensity fraction of the ith lifetime component τ_i.
[b] S.D. value is ±0.1 ns.
[c] The anisotropies $r(t)$ were analyzed for a series of exponentials by a model-independent maximum entropy method without setting assumptions about the shape of the correlation time distributions (50), $r(t) = \Sigma_i \beta_i \exp(-t/\phi_i)$, where amplitudes β_i represent the distribution of the correlation times ϕ_i.
[d] This mutant was prepared by mutating Trp-770, Trp-865 to Phe and Phe-823 to Trp.
[e] This mutant was prepared by mutating Trp-865 to Phe.

Enzyme Activity Measurements—The enzymatic activity of ASK1-CD was examined using [γ-^{32}P]ATP assay with purified human MKK4 K131A as a specific substrate. The reaction volume of 45 μl consisted of 200 nM pASK1-CD or the 14-3-3 binding-defective mutant pASK1-CD S966A, 2.7 μM MKK4, and 70 μM 14-3-3ζΔC protein (where needed) in 50 mM Tris-HCl (pH 7.5), 150 mM NaCl, 20 mM $MgCl_2$, 5 mM DTT. The used concentration of 14-3-3ζΔC should allow for saturation of pASK1-CD considering the K_D value of 4 ± 2 μM. The reaction was performed at 30 °C and initiated by an addition of 5 μl of 2.5 mM [γ-^{32}P]ATP (PerkinElmer Life Sciences) to a final ATP concentration 250 μM (~2.5 μCi per reaction). After a 2.5-h incubation at 30 °C, the reaction was stopped by spotting 40 μl of the reaction mixture onto a P81 phosphocellulose paper strip (Millipore) and washing in 3 × 800 ml of 75 mM phosphoric acid 10 min each. Strips were dried and inserted into vials containing 5 ml of scintillation fluid (Rotiszint™, Carl Roth). Counts were measured using Quantasmart™ liquid analyzer (PerkinElmer Life Sciences). The time dependence of product formation confirmed that the data were obtained under linear conditions of the assay.

AUC—SV Experiments Were Performed Using a ProteomLab™ XL-I Analytical Ultracentrifuge (Beckman Coulter) as described previously (37). Briefly, samples were dialyzed against buffer containing 50 mM Tris-HCl (pH 7.5), 200 mM NaCl, and 2 mM 2-mercaptoethanol before analysis. All sedimentation profiles were recorded with absorption optics at 42 000 rpm. The diffusion-deconvoluted sedimentation coefficient distributions $c(s)$ were calculated from raw data using the package SEDFIT (38). SV AUC analysis of mixtures of pASK1-CD and 14-3-3ζ (WT or ΔC mutant) at various molar ratios was performed with 18 μM pASK1-CD and 1.8–180 μM 14-3-3ζ. Obtained data were fitted, and apparent K_D was estimated using the global Lamm equation modeling with a 1:1 Langmuir binding model implemented in the SEDPHAT software (39).

SAXS—SAXS data were collected on the European Molecular Biology Laboratory (EMBL) P12 beamline on the storage ring PETRA III (Deutsches Elektronen Synchrotron (DESY), Hamburg, Germany). The SAXS measurements were conducted in buffer containing 50 mM Tris-HCl (pH 7.5), 200 mM

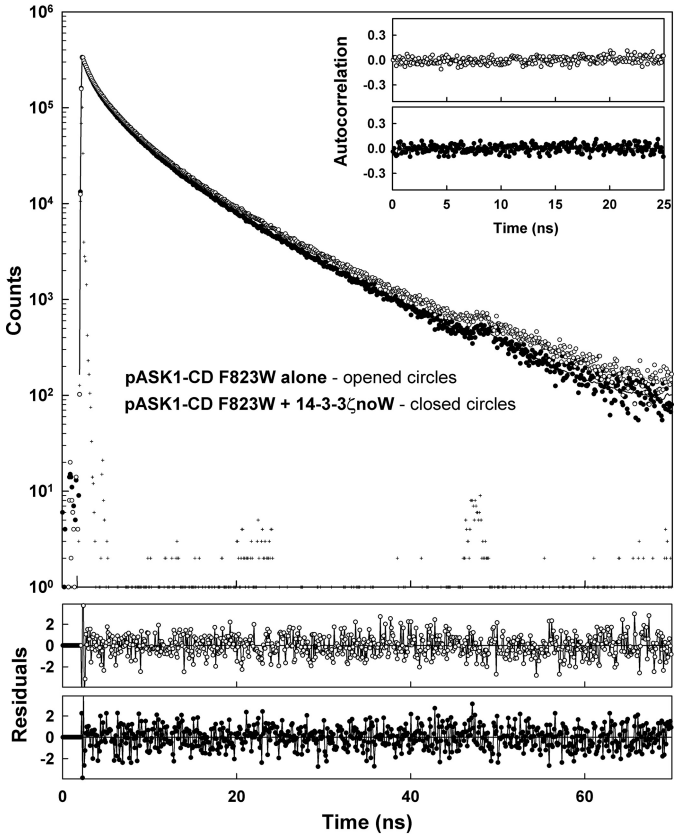

FIGURE 9. **Time-resolved tryptophan fluorescence measurements of pASK1-CD containing single tryptophan, Trp-823.** Share are normalized fluorescence intensity decays of pASK1-CD mutant containing a single tryptophan, Trp-823, in the absence (*open circles*) and presence (*closed circles*) of 14-3-3ζnoW. Raw data clearly show significant shortening of the decay in the presence of 14-3-3ζnoW, as the difference between the two decays is visibly above the data noise level. + denotes instrument response function.

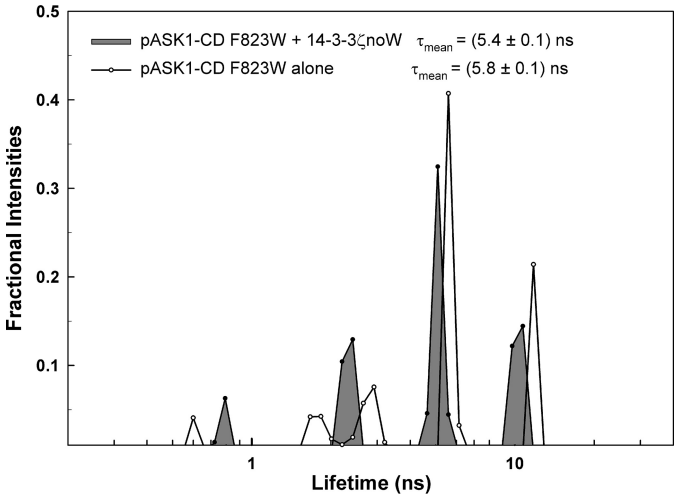

FIGURE 10. **Excited state lifetime distribution of pASK1-CD Trp-823.** Excited state lifetime distribution of pASK1-CD mutant containing single tryptophan Trp-823 in the absence (*unfilled distribution*) and the presence of 14-3-3ζnoW (*gray-filled distribution*). As can be noticed, the two longest lifetime peaks dominating the mean excited state lifetime become shortened upon the 14-3-3ζnoW binding. As a consequence, τ_{mean} of Trp-823 is reduced. *Errors* represent the S.D.

NaCl, 1 mM EDTA, and 2 mM DTT. The ASK1-CD concentrations were 4.1–9.1 mg·ml^{-1}, the 14-3-3ζΔC concentrations were 7.7–17.4 mg·ml^{-1}, and the pASK1-CD·14-3-3ζΔC complex (2:2 molar stoichiometry) concentrations were 7.7–17.6 mg·ml^{-1}. The forward scattering $I(0)$ and the radius of gyration R_g were calculated using the Guinier approximation for the s ($s = 4\pi\sin(\theta)/\lambda$, where 2θ is the scattering angle, and λ is the wavelength) range, which satisfies the $sR_g < 1.3$ condition (40). The distance distribution functions $P(r)$ and the maximum particle dimensions D_{max} were computed using the program GNOM (41). The solute apparent molecular mass (MM_{exp}) was estimated by comparing the forward scattering with that from reference solutions of bovine serum albumin. The excluded volume of the hydrated particle (the Porod volume, V_p) was computed using the program PRIMUS (42). The program DAMMIF (43) was used to calculate *ab initio* molecular envelopes. Multiple iterations of DAMMIF were averaged using the program DAMAVER (44). Calculated molecular envelopes were aligned to structural models using the program SUPCOMB (45). Theoretical scattering curves were calculated from structural models and fitted to experimental scattering data using the programs CRYSOL (46) and FoXS (47).

Structural Modeling of the pASK1-CD·14-3-3ζ Complex Using SAXS and Cross-linking Data—The AllosMod-FoXS web server was used to prepare models of ASK1-CD and the ASK1-CD·14-3-3ζ complex as well as to generate their alternate conformations consistent with the experimental SAXS data (22, 23). The model of ASK1-CD (659–973) was prepared using the crystal structure of the kinase domain of ASK1 (670–940) (48). The starting model of the complex was prepared using the model of ASK1-CD and the crystal structure of 14-3-3ζ (21). The C-terminal 14-3-3 binding motif of ASK1 containing Ser-966 (sequence ^{963}RSISLP^{968}) was restrained in the ligand binding groove of 14-3-3ζ in the orientation observed in structures of 14-3-3 with bound ligands (13, 17, 21). Simulations consisting of 10–30 runs (generating 101 conformations for each run) were allowed to sample the most probable conformations consistent with the starting structures and used distances derived from intermolecular cross-links (Table 3, cross-links #1–4) restrained to 20 ± 8 Å from Cα to Cα. Multistate modeling of the pASK1-CD·14-3-3ζ complex was performed using the MultiFoXS web server with the same starting structure (24, 47). The ASK1-CD regions 659–669 and 941–973 (with the exception of restrained 14-3-3 binding motif of one ASK1-CD protomer, region 963–968) were defined as flexible regions. The simulation generated 10,000 conformations that were used to interpret the SAXS data.

Chemical Cross-linking—Equimolar mixtures of both pASK1-CD and ASK1-CD with 1433ζΔC were cross-linked using cross-linking agent bis(sulfosuccinimidyl)glutarate (BS^{2}G) to identify intermolecular cross-links at the binding interface. Cross-linking reactions were performed with 80 μM protein solutions in buffer containing 10 mM HEPES (pH 7.5), 200 mM NaCl, 0.1 mM TCEP (tris(2-carboxyethyl)phosphine). Reactions were started by adding freshly prepared stock solution of BS^{2}G (10 mg·ml^{-1}) in a 50× molar excess to protein solutions, and reactions were incubated for 2 h at room temperature. After cross-linking, proteins were separated on a reducing NuPAGE 4–12% Bis-Tris gel using MES running buffer, and the bands corresponding to both a monomeric and a dimeric cross-linked protein were excised and analyzed for intermolec-

ular cross-links using high resolution MS as described previously (49). All identified cross-links were manually checked in the raw data to remove false positives.

NMR Measurements—The ^{31}P NMR spectra with proton decoupling were measured on a Bruker AVANCE III instrument (^{1}H at 500.0 MHz and ^{31}P at 202.4 MHz) equipped with a 5-mm BBO CryoProbe. Phosphoric acid (85%) was used as external standard of ^{31}P chemical shifts. Typical experimental conditions for the ^{31}P spectra were 10,000 scans, with a spectral width of 400 ppm and an acquisition time of 0.4 s, yielding 64,000 data points. The repetition delay of 2 s led to the total measurement time of ~6 h per spectrum. The Lorenzian broadening by 20 Hz was applied in processing. Experiments were recorded at 23 °C on samples containing 100–200 μM pASK1-CD (or the 14-3-3 binding-defective mutant pASK1-CD S966A) and 500–900 μM 14-3-3ζΔC dissolved in 50 mM Tris-HCl (pH 7.5), 200 mM NaCl, 1 mM EDTA, 5 mM DTT, 10% (w/v) glycerol, and 10% (v/v) D_2O. The resulting spectra had signal-to-noise ratio in the range of 20–80.

Time-resolved Fluorescence Measurements—Time-resolved fluorescence intensity and anisotropy decay measurements as well as data analysis were performed as has been described previously (37). Tryptophan emission was excited at 298 nm by a tripled output of the Ti:Sapphire laser. Tryptophan fluorescence was isolated at 355 nm by a combination of monochromator and a stack of UG1 and BG40 glass filters (Thorlabs) placed in front of the input slit. Samples were placed in a thermostatic holder, and all experiments were performed at 23 °C in buffer containing 50 mM Tris-HCl (pH 7.5), 200 mM NaCl, 1 mM EDTA, 5 mM DTT, 10% (w/v) glycerol, and 0.05% (w/v) Nonidet P-40. The pASK1-CD and 14-3-3ζnoW concentrations were 15 and 110 μM, respectively.

Author Contributions—O. P. and D. K. conducted most of the experiments, analyzed the results, and edited the manuscript. Z. K. and Z. T. helped O. P. and D. K. with conducting the experiments and editing the manuscript. P. M. performed LC-MS analyses. P. H. and J. V. performed time-resolved fluorescence experiments, data analysis, and interpretation, and P. H. helped with editing the manuscript. V. O. and T. O. conceived the idea for the project, analyzed the results, and wrote the manuscript.

Acknowledgments—We thank Petr Novak for assistance with MS, Martin Dracinsky for assistance with NMR, and Daniel Steiner for critical reading of the manuscript. Access to the MS facility was enabled by the EU project CZ.1.05/1.1.00/02.0109 and by the Czech Infrastructure for Integrative Structural Biology (LM2015043).

References

1. Shiizaki, S., Naguro, I., and Ichijo, H. (2013) Activation mechanisms of ASK1 in response to various stresses and its significance in intracellular signaling. *Adv. Biol. Regul.* **53,** 135–144
2. Kawarazaki, Y., Ichijo, H., and Naguro, I. (2014) Apoptosis signal-regulating kinase 1 as a therapeutic target. *Expert Opin Ther Targets* **18,** 651–664
3. Noguchi, T., Takeda, K., Matsuzawa, A., Saegusa, K., Nakano, H., Gohda, J., Inoue, J., and Ichijo, H. (2005) Recruitment of tumor necrosis factor receptor-associated factor family proteins to apoptosis signal-regulating kinase 1 signalosome is essential for oxidative stress-induced cell death. *J. Biol. Chem.* **280,** 37033–37040
4. Cockrell, L. M., Puckett, M. C., Goldman, E. H., Khuri, F. R., and Fu, H. (2010) Dual engagement of 14-3-3 proteins controls signal relay from ASK2 to the ASK1 signalosome. *Oncogene* **29,** 822–830
5. Saitoh, M., Nishitoh, H., Fujii, M., Takeda, K., Tobiume, K., Sawada, Y., Kawabata, M., Miyazono, K., and Ichijo, H. (1998) Mammalian thioredoxin is a direct inhibitor of apoptosis signal-regulating kinase (ASK) 1. *EMBO J.* **17,** 2596–2606
6. Zhang, L., Chen, J., and Fu, H. (1999) Suppression of apoptosis signal-regulating kinase 1-induced cell death by 14-3-3 proteins. *Proc. Natl. Acad. Sci. U.S.A.* **96,** 8511–8515
7. Goldman, E. H., Chen, L., and Fu, H. (2004) Activation of apoptosis signal-regulating kinase 1 by reactive oxygen species through dephosphorylation at serine 967 and 14-3-3 dissociation. *J. Biol. Chem.* **279,** 10442–10449
8. Fujino, G., Noguchi, T., Matsuzawa, A., Yamauchi, S., Saitoh, M., Takeda, K., and Ichijo, H. (2007) Thioredoxin and TRAF family proteins regulate reactive oxygen species-dependent activation of ASK1 through reciprocal modulation of the N-terminal homophilic interaction of ASK1. *Mol. Cell. Biol.* **27,** 8152–8163
9. Muslin, A. J., Tanner, J. W., Allen, P. M., and Shaw, A. S. (1996) Interaction of 14-3-3 with signaling proteins is mediated by the recognition of phosphoserine. *Cell* **84,** 889–897
10. Freeman, A. K., and Morrison, D. K. (2011) 14-3-3 Proteins: diverse functions in cell proliferation and cancer progression. *Semin. Cell Dev. Biol.* **22,** 681–687
11. Gardino, A. K., and Yaffe, M. B. (2011) 14-3-3 proteins as signaling integration points for cell cycle control and apoptosis. *Semin Cell Dev. Biol.* **22,** 688–695
12. Klein, D. C., Ganguly, S., Coon, S. L., Shi, Q., Gaildrat, P., Morin, F., Weller, J. L., Obsil, T., Hickman, A., and Dyda, F. (2003) 14-3-3 proteins in pineal photoneuroendocrine transduction: how many roles? *J. Neuroendocrinol.* **15,** 370–377
13. Obsil, T., Ghirlando, R., Klein, D. C., Ganguly, S., and Dyda, F. (2001) Crystal structure of the 14-3-3ζ:serotonin N-acetyltransferase complex. a role for scaffolding in enzyme regulation. *Cell* **105,** 257–267
14. Kopecka, M., Kosek, D., Kukacka, Z., Rezabkova, L., Man, P., Novak, P., Obsil, T., and Obsilova, V. (2014) Role of the EF-hand-like motif in the 14-3-3 protein-mediated activation of yeast neutral trehalase Nth1. *J. Biol. Chem.* **289,** 13948–13961
15. Kleppe, R., Rosati, S., Jorge-Finnigan, A., Alvira, S., Ghorbani, S., Haavik, J., Valpuesta, J. M., Heck, A. J., and Martinez, A. (2014) Phosphorylation dependence and stoichiometry of the complex formed by tyrosine hydroxylase and 14-3-3γ. *Mol. Cell. Proteomics* **13,** 2017–2030
16. Yip-Schneider, M. T., Miao, W., Lin, A., Barnard, D. S., Tzivion, G., and Marshall, M. S. (2000) Regulation of the Raf-1 kinase domain by phosphorylation and 14-3-3 association. *Biochem. J.* **351,** 151–159
17. Ottmann, C., Marco, S., Jaspert, N., Marcon, C., Schauer, N., Weyand, M., Vandermeeren, C., Duby, G., Boutry, M., Wittinghofer, A., Rigaud, J. L., and Oecking, C. (2007) Structure of a 14-3-3 coordinated hexamer of the plant plasma membrane H+ -ATPase by combining x-ray crystallography and electron cryomicroscopy. *Mol. Cell* **25,** 427–440
18. Kacirova, M., Kosek, D., Kadek, A., Man, P., Vecer, J., Herman, P., Obsilova, V., and Obsil, T. (2015) Structural characterization of phosducin and its complex with the 14-3-3 protein. *J. Biol. Chem.* **290,** 16246–16260
19. Petoukhov, M. V., Franke, D., Shkumatov, A. V., Tria, G., Kikhney, A. G., Gajda, M., Gorba, C., Mertens, H. D., Konarev, P. V., and Svergun, D. I. (2012) New developments in the program package for small-angle scattering data analysis. *J. Appl. Crystallogr.* **45,** 342–350
20. Receveur-Brechot, V., and Durand, D. (2012) How random are intrinsically disordered proteins? A small angle scattering perspective. *Curr. Protein Pept. Sci.* **13,** 55–75
21. Rittinger, K., Budman, J., Xu, J., Volinia, S., Cantley, L. C., Smerdon, S. J., Gamblin, S. J., and Yaffe, M. B. (1999) Structural analysis of 14-3-3 phosphopeptide complexes identifies a dual role for the nuclear export signal of 14-3-3 in ligand binding. *Mol. Cell* **4,** 153–166
22. Weinkam, P., Pons, J., and Sali, A. (2012) Structure-based model of allostery predicts coupling between distant sites. *Proc. Natl. Acad. Sci. U.S.A.* **109,** 4875–4880

23. Schneidman-Duhovny, D., Hammel, M., and Sali, A. (2010) FoXS: a web server for rapid computation and fitting of SAXS profiles. *Nucleic Acids Res.* **38,** W540–W544
24. Raveh, B., Enosh, A., Schueler-Furman, O., and Halperin, D. (2009) Rapid sampling of molecular motions with prior information constraints. *PLoS Comput. Biol.* **5,** e1000295
25. Carter, L., Kim, S. J., Schneidman-Duhovny, D., Stöhr, J., Poncet-Montange, G., Weiss, T. M., Tsuruta, H., Prusiner, S. B., and Sali, A. (2015) Prion protein-antibody complexes characterized by chromatography-coupled small-angle x-ray scattering. *Biophys. J.* **109,** 793–805
26. Bock, J. L., and Sheard, B. (1975) ^{31}P NMR of alkaline phosphatase. *Biochem. Biophys. Res. Commun.* **66,** 24–30
27. Silhan, J., Obsilova, V., Vecer, J., Herman, P., Sulc, M., Teisinger, J., and Obsil, T. (2004) 14-3-3 protein C-terminal stretch occupies ligand binding groove and is displaced by phosphopeptide binding. *J. Biol. Chem.* **279,** 49113–49119
28. Lakowicz, J. R. (1999) *Principles of Fluorescence Spectroscopy*, 2nd Ed., pp. 129–345, Kluwer Academic/Plenum Publishers, New York
29. Johnson, M. L. (2008) Nonlinear least-squares fitting methods. *Methods Cell Biol.* **84,** 781–805
30. Durand, D., Cannella, D., Dubosclard, V., Pebay-Peyroula, E., Vachette, P., and Fieschi, F. (2006) Small-angle x-ray scattering reveals an extended organization for the autoinhibitory resting state of the p47(phox) modular protein. *Biochemistry* **45,** 7185–7193
31. Acuner Ozbabacan, S. E., Engin, H. B., Gursoy, A., and Keskin, O. (2011) Transient protein-protein interactions. *PEDS* **24,** 635–648
32. Jeffrey, P. D., Russo, A. A., Polyak, K., Gibbs, E., Hurwitz, J., Massagué, J., and Pavletich, N. P. (1995) Mechanism of CDK activation revealed by the structure of a cyclinA-CDK2 complex. *Nature* **376,** 313–320
33. Kim, C., Xuong, N. H., and Taylor, S. S. (2005) Crystal structure of a complex between the catalytic and regulatory (RIα) subunits of PKA. *Science* **307,** 690–696
34. White, A., Pargellis, C. A., Studts, J. M., Werneburg, B. G., and Farmer, B. T. (2007) Molecular basis of MAPK-activated protein kinase 2:38 assembly. *Proc. Natl. Acad. Sci. U.S.A.* **104,** 6353–6358
35. Seong, H. A., Jung, H., Ichijo, H., and Ha, H. (2010) Reciprocal negative regulation of PDK1 and ASK1 signaling by direct interaction and phosphorylation. *J. Biol. Chem.* **285,** 2397–2414
36. Hari, S. B., Merritt, E. A., and Maly, D. J. (2013) Sequence determinants of a specific inactive protein kinase conformation. *Chem. Biol.* **20,** 806–815
37. Kosek, D., Kylarova, S., Psenakova, K., Rezabkova, L., Herman, P., Vecer, J., Obsilova, V., and Obsil, T. (2014) Biophysical and structural characterization of the thioredoxin-binding domain of protein kinase ASK1 and its interaction with reduced thioredoxin. *J. Biol. Chem.* **289,** 24463–24474
38. Schuck, P. (2000) Size-distribution analysis of macromolecules by sedimentation velocity ultracentrifugation and lamm equation modeling. *Biophys. J.* **78,** 1606–1619
39. Dam, J., Velikovsky, C. A., Mariuzza, R. A., Urbanke, C., and Schuck, P. (2005) Sedimentation velocity analysis of heterogeneous protein-protein interactions: Lamm equation modeling and sedimentation coefficient distributions c(s). *Biophys. J.* **89,** 619–634
40. Guinier, A. (1939) La diffraction des rayons X aux très faibles angles: applications à l'etude des phénomènes ultra-microscopies. *Ann. Phys.-Paris* **12,** 161–237
41. Svergun, D. I. (1992) Determination of the regularization parameter in indirect-transform methods using perceptual criteria. *J. Appl. Crystallogr.* **25,** 495–503
42. Konarev, P. V., Volkov, V. V., Sokolova, A. V., Koch, M. H. J., and Svergun, D. I. (2003) PRIMUS: a Windows PC-based system for small-angle scattering data analysis. *J. Appl. Crystallogr.* **36,** 1277–1282
43. Franke, D., and Svergun, D. I. (2009) DAMMIF, a program for rapid *ab initio* shape determination in small-angle scattering. *J. Appl. Crystallogr.* **42,** 342–346
44. Volkov, V. V., and Svergun, D. I. (2003) Uniqueness of ab initio shape determination in small-angle scattering. *J. Appl. Crystallogr.* **36,** 860–864
45. Kozin, M. B., and Svergun, D. I. (2001) Automated matching of high and low resolution structural models. *J. Appl. Crystallogr.* **34,** 33–41
46. Svergun, D., Barberato, C., and Koch, M. H. J. (1995) CRYSOL: a program to evaluate x-ray solution scattering of biological macromolecules from atomic coordinates. *J. Appl. Crystallogr.* **28,** 768–773
47. Schneidman-Duhovny, D., Hammel, M., Tainer, J. A., and Sali, A. (2013) Accurate SAXS profile computation and its assessment by contrast variation experiments. *Biophys. J.* **105,** 962–974
48. Bunkoczi, G., Salah, E., Filippakopoulos, P., Fedorov, O., Müller, S., Sobott, F., Parker, S. A., Zhang, H., Min, W., Turk, B. E., and Knapp, S. (2007) Structural and functional characterization of the human protein kinase ASK1. *Structure* **15,** 1215–1226
49. Macakova, E., Kopecka, M., Kukacka, Z., Veisova, D., Novak, P., Man, P., Obsil, T., and Obsilova, V. (2013) Structural basis of the 14-3-3 protein-dependent activation of yeast neutral trehalase Nth1. *Biochim. Biophys. Acta* **1830,** 4491–4499
50. Vecer, J., and Herman, P. (2011) Maximum entropy analysis of analytically simulated complex fluorescence decays. *J. fluoresc.* **21,** 873–881